KSME

Springer

Journal of Mechanical Science and Technology 35 (8) 2021

Original Article
DOI 10.1007/s12206-021-0735-5

Keywords:
· Incremental forming
· Multi-stage forming
· Selective forming
· Forming angle

Correspondence to:
Hu Zhu
zhuhu10@163.com

Citation:
Zhu, H., Liu, L., Liu, Y., Kang, J. (2021). Research on the selective multi-stage two point incremental forming based on the forming angle. Journal of Mechanical Science and Technology 35 (8) (2021) 3643~3658.
http://doi.org/10.1007/s12206-021-0735-5

Received February 12th, 2021
Revised April 5th, 2021
Accepted April 20th, 2021

† Recommended by Editor Hyung Wook Park

© The Korean Society of Mechanical Engineers and Springer-Verlag GmbH Germany, part of Springer Nature 2021

Research on the selective multi-stage two point incremental forming based on the forming angle

Hu Zhu[1], Luteng Liu[1], Yibo Liu[2] and Jaeguan Kang[3]

[1]College of Mechanical and Electrical Engineering, Shenyang Aerospace University, Shenyang, Liaoning 110136, China, [2]Science and Technology Training Center, Guidaojiaotong Polytechnic Institute, Shenyang 110023, China, [3]School of Mechanical and Automation Engineering, Kyungnam University, Changwon 51767, Korea

Abstract For sheet metal parts with the vertical-wall partially and irregularly distributed on the sides (VWPIS) that contains both the difficult-form-surface (i.e., vertical-wall) with large forming angle and easy-to-form surface (i.e., gently tilted surface) with small forming angle, a selective multi-stage two point incremental forming (SMTPIF) on the basis of the forming angle was proposed. This SMTPIF method performs multi-stage forming only for the difficult-form-surface and gives different forming strategies and forming parameters to the different surface regions according to the forming angle. The algorithms for surface zoning, generation of the small forming angle surface for vertical-wall, generation of one-stage forming model by combining the easy-form-surface and small forming angle surface were presented. Meanwhile, the algorithm for the generation of the toolpath that is suitable to the SMTPIF was also given. The effectiveness of the proposed algorithm and the SMTPIF was verified by using the case studies, the finite element analysis, and the forming experiments. The results indicate that the SMTPIF can fabricate the VWPIS with short forming time and no sinking phenomenon.

1. Introduction

Sheet metal incremental forming (IF) is a dieless forming process developed under the basis of rapid prototyping, which can quickly and economically fabricate the sheet metal part without expensive dies. So it can be applied to multi variety and less batch production.

The important problem to be solved in the IF is vertical-wall part forming. Because the vertical-wall part has surfaces with large forming angle that exceeds the forming limit angle θ_{lim}, it cannot be formed directly by conventional one-stage forming. According to the distribution of the vertical-wall, the common vertical-wall model can be divided as a model with a vertical-wall on all sides (VWAS, Fig. 1(a)), a model with a vertical-wall on all sides and complex cross-section (VWAS & CCS, Fig. 1(b)), a model with a vertical-wall and only on one side (VWOS, Fig. 1(c)), a model with the vertical-wall partially and irregularly on the sides (VWPIS, Fig. 1(d)). Researchers have developed various forming methods according to the different characteristics of vertical wall models.

Up to now, multi-stage incremental forming (MIF) has the most widely used method for vertical-wall models. The studies on the MIF are mainly concentrated on the forming strategy, toolpath planning, rigid body translation, forming formability, and geometrical accuracy.

Kim et al. [1] proposed a two-stage forming strategy to improve the formability of incremental forming and found through experiments that the construction method for the intermediate models based on the thickness strain analysis can effectively improve the thickness distribution. Iseki et al. [2] designed a manual forming device to form vertical-walled rectangular shallow shells with multiple tools in multiple stages and the formed straight-walled rectangular shallow shells have better contour performance. Hirt et al. [3] proposed a gradually increasing angle strategy of MIF using convex die and realized the forming of the square cone with the wall

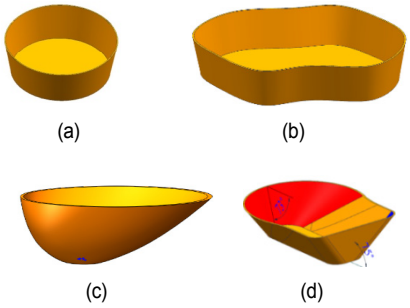

Fig. 1. Vertical-wall part types: (a) VWAS; (b) VWAS and CCS; (c) VWOS; (d) VWPIS.

angles of 81° through experiments.

Although the formation of vertical-wall parts can be achieved by MIF, there is an obvious defect in that the formed sheet parts have obvious step features (Skjoedt [4] and Duflou [5]) at the bottom, which has a great influence on the accuracy. For the step feature occurring in MIF, Malhotra et al. [6] attributed the occurrence of the step feature to rigid body motion (RBM) and predicted the RBM in MIF, and then developed a toolpath strategy combined in-to-out (IO) and out-to-in (OI) toolpaths to slow this phenomenon. And in the research of Duflou [5], the RBM can also clearly seen in the unformed area from the figure of material flows in the MIF. Lingam et al. [7] predicted the geometric shape of the parts formed by MIF considering the elastic deflection of the sheet and the tool, and verified the feasibility of the prediction method through experiments. The method has better contour fit compared with the prediction method that only considers the RBM, but this method is only suitable for axisymmetric parts. Ndip-Agbor et al. [8] were no longer limited to analysis on two-dimensional cross-sections, and used the 3D contact patch to analyze and predict the RBM in MIF.

On the other hand, the deformation form of the material in MIF is more complicated than that in one-stage forming, which makes it more difficult to predict and analyze the thickness in MIF. Suresh et al. [9] analyzed the four-stage forming process of the 85° truncated cone using FE analysis and found that the strain of the sheet in the multi-stage forming tends to be biaxially stretched. Mirnia et al. [10] established a numerical analysis model suitable for incremental forming based on forming limit analysis, which has higher calculation efficiency compared with the commercial finite element software and its reliability was also verified by experiments.

In the aspect of thickness prediction, under the assumption that the material flows along the normal line of the current geometry shape, Cao et al. [11] established a thickness prediction model based on material point backtracking based on the prediction of the cross-section geometry. The experiments showed that the sheet thickness prediction of the simple rotating body in MIF can be achieved. Li et al. [12] analyzed the effect of toolpath strategy on the thickness distribution by taking a square cone as the research object and obtained the best multi-stage forming strategy by comparing the thickness distribution of the different strategies. Li et al. [13] established a theoretical model of thickness distribution that is suitable for MIF and adopted three path strategies of MIF to study the effect of the paths on thickness distribution.

To obtain better quality of formed parts, scholars are also constantly exploring new strategies and methods to form straight wall parts. Liu et al. [14] developed an open-loop analysis model based on thickness strain and established a closed-loop multi-stage design method for simple bodies. Gupta et al. [15] analyzed four strategies of MIF through experiment and successfully fabricated the C-channel parts used in aerospace by using the conventional downward strategy. They found that variable angles of intermediate forming help to improve the thickness distribution. Tanaka [16] proposed a special intermediate model construction method for the vertical-wall square box, which divides the square box into multiple square cones and controls the direction of the path planes of each square cone. Wu et al. [17] made improvements on the basis of the IO strategy, and verified its effectiveness in optimizing thickness distribution and reducing bottom subsidence through experiments and FE. Gianluca et al. [18] adopted different strategies of MIF to form the vertical-wall square box, and found that the non-horizontal path strategy has better formability and special material redistribution for the vertical-wall square box. Dai et al. [19] used three-pass forming method combined with path compensation to form the sheet metal parts with step features and reduced the geometric error of the sheet metal part.

But the research objects of the above studies on the MIF are mainly concentrated on a regular simple body such as tubes, pyramid, square boxes or cylinder (displayed in Fig. 1(a)). For the problem, Zhu et al. [20] proposed a virtual auxiliary body based MIF that is specifically used for the forming of the VWAS and CCS by multi-directionally orienting the sheet postures, which can form the VWAS & CCS with good contour accuracy and relatively uniform thickness distribution.

However, the above studies are still aimed at sheet metal parts with a vertical-wall on all sides, shown as Figs. 1(a) and (b). For the sheet metal parts with both vertical-walls and easy-to-form surfaces (Figs. 1(c) and (d)), the applicability of the currently established prediction and analysis models cannot be determined due to the influence of the easy-to-form surface. At present, most of the researches on sheet metal parts with partial vertical-walls are focused on the VWOS (Fig. 1(c)). Zhu and Li [21] reviewed the existing methods for fabricating the VWOS by tilting the workplane or toolpath from the difficult-form-surface to the easy-form-surface, and pointed out that the existing approaches (i.e., the inclined model or one-way inclined toolpath) are only limited to the VWOS and cannot be applied to the VWPIS (Fig. 1(d)).

The VWPIS is more difficult to form than other types, because it has partially and irregularly distributed difficult-to-form surface and the easy-to-form surface. For example, in the research on the taillight bracket forming by Li et al. [22], it

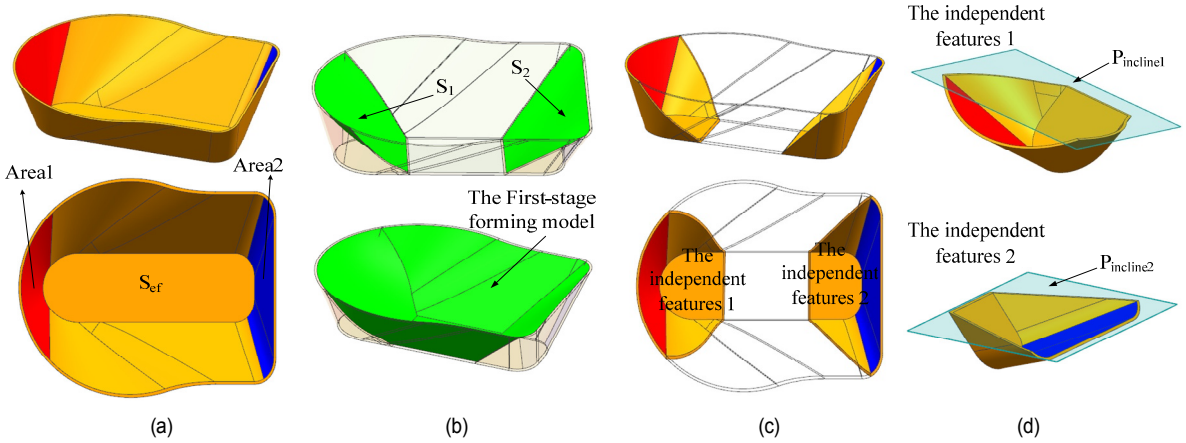

Fig. 2. General idea.

could be found that the intermediate model constructing process of the VWPIS was very complicated, and the forming parameters need to be determined through multiple experiments, which will undoubtedly greatly increase forming time and material costs.

However, the multiple repeated forming process of the traditional MIF causes problems such as low forming efficiency, material hardening, and step features. Therefore, for the VWPIS that is not completely composed of the vertical-walls, i.e., composed of both the vertical-wall and the easy-to-form surface that are partially and irregularly distributed on the sides, it is not necessary to form all surfaces using the MIF, but selectively only perform the MIF on the vertical-wall and form the easy-to-form surface using one-stage forming.

This paper proposes a method of selective multi-stage two point incremental forming (SMTPIF) that distinguishes the surfaces of the VWPIS into difficult-to-form surfaces and easy-to-form surfaces based on the forming angle and forms the difficult-to-form surfaces and the easy-to-form surfaces by using the MIF and one-stage forming, respectively. The proposed SMTPIF combines the ideas of local multi-stage forming and sheet posture adjustment method so as to avoid the complicated construction process of the intermediate model in the traditional MIF and also overcome the problems (such as step features, low efficiency) in the traditional MIF.

2. General idea

The general idea of the SMTPIF is described by using the VWPIS model (Fig. 2). In this model, the vertical-wall surfaces with maximum forming angles of 73° and 75° are respectively and irregularly distributed in the red (Area 1) and blue areas (Area 2), and the other surfaces are easy-to-form surfaces S_{ef} with small forming angles. In the proposed approach, one-stage forming is used to form the easy-to-form surfaces that are to be used as one of the components of first-stage forming model. And multi-stage forming is adopted for the vertical-wall areas. First, the surface S_i (i = 1, 2,…, n) with small forming angle is constructed for each vertical-wall surface as another component of the first-stage forming model and merged with the existing easy-to-form surface to constitute the first-stage forming model (Fig. 2(b)).

After the first-stage forming process, the sheet surface of the vertical-wall area is converted from horizontal to the inclined surface with the small forming angle S_i, and the forming angle of the vertical -wall surface relative to the new sheet surface is reduced, which lays the foundation for the second stage forming. Then, the remaining unformed areas after the first-stage forming are taken as the independent features for the second stage forming, as shown in Fig. 2(c). The second stage forming method for each independent feature is to select an inclined plane $P_{incline}$ so that the forming angle of the independent features relative to the $P_{incline}$ is less than θ_{lim} to ensure that the independent feature can be successfully formed.

If no inclined plane that makes the relative forming angle of the independent feature to be smaller than the θ_{lim} can be found, then the independent feature (as shown in Fig. 2(d)) will be regarded as a new VWPIS to repeat the steps shown in Figs. 2(a) and (b), which is continued to construct a small forming angled surface (relative to the slicing plane $P_{slicing}$) S'_i to perform the second stage forming. Then, for the obtained unformed independent features of the current model, the inclined sheet surface $P'_{incline}$ is reselected so that the forming angle with respect to $P'_{incline}$ is smaller than the θ_{lim}. Through the steps mentioned above, the VWPIS can be formed by the SMTPIF.

The second stage and the subsequent stage forming for the vertical-wall area 1 and area 2 are separately and independently performed forming processes, as shown in Fig. 2(d).

In this way, the different forming strategies and forming parameters can be used for the different regions with different forming angles, which makes it possible to reduce the occurrence of sinking, improve the forming efficiency, and avoid the material hardening caused by the multiple forming process in the conventional multi-stage forming.

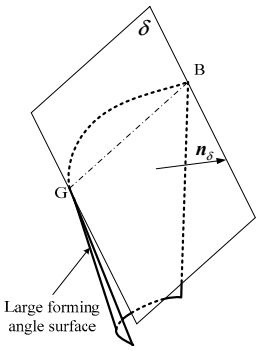

Fig. 3. The slicing plane δ.

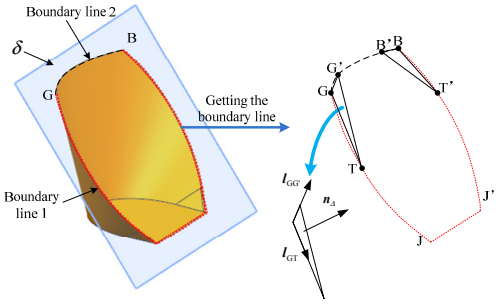

Fig. 4. Segmentation of the boundary line.

3. First-stage forming

3.1 Construction of first-stage forming model

3.1.1 Extraction of surfaces with large forming angle and zoning

First, the internal surface of the part to be formed is extracted using the normal vector of the triangular faces. Then, the extracted surface is offset a distance of tool radius along the direction of the normal vector using the vertex offset method to generate the tool location face (TLF), and extract boundary line of the TLF. Next, the forming angle of each triangular patch relative to the horizontal plane is found through the normal vector of the triangular patch and the horizontal plane. Finally, the surface is zoned according to whether the forming angle θ_i is greater than $\theta_{\lim}$. Meanwhile, the triangular faces with the large forming angle are further divided according to whether the triangular faces are connected to each other, and the boundary line of the large forming angle area is extracted.

3.1.2 Generation of the small forming angle surface S_i for the large forming angle surface

First, an inclined slicing plane δ (inclination angle θ_δ is smaller than the $\theta_{\lim}$) is used to cut the easy-to-form area to obtain the boundary line of the small forming angle surface to be generated. Then, the boundary line is segmented and the triangular meshing method is used to generate the small forming angle surfaces.

1) The slicing plane determination

The two points B (x_B, y_B, z_B) and G (x_G, y_G, z_G) at the top of the boundary line of the large forming angle area are extracted, and then the direction vector $\boldsymbol{l}_{BG}=(a,b,c)=(x_G-x_B,y_G-y_B,z_G-z_B)$ of the BG could be obtained (Fig. 3). The plane beam equation passing through the BG is as follows.

$$b(x-x_B)+(uc-a)(y-y_B)-ub(z-z_B)=0\,. \tag{1}$$

Among them, u is the coefficient of the plane beam formula. If the normal vector of any slicing plane δ in the plane beam is expressed as $\boldsymbol{n}_\delta=(x_\delta,y_\delta,z_\delta)=(b,uc-a,-ub)$ and the normal vector of the horizontal plane is expressed as $\boldsymbol{n}_o=(0,0,1)$, then the included angle θ_δ between the slicing plane δ and the horizontal plane is as follows.

$$\cos\theta_\delta=\frac{n_\delta n_o}{|n_\delta||n_o|}\,. \tag{2}$$

So, the plane beam coefficient u is as follows.

$$u=\frac{2t^2ac\pm\sqrt{(2t^2ac)^2-4(t^2b^2+t^2c^2-b^2)(t^2a^2+t^2b^2)}}{2(t^2b^2+t^2c^2-b^2)}\,. \tag{3}$$

Among them, $t=\cos\theta_\delta$ and $ub>0$. In this way, the slicing plane δ can be determined by setting θ_δ, and the value of θ_δ should be less than the $\theta_{\lim}$.

2) Slicing the easy-to-form area

The slicing process of the easy-to-form area is the intersection of the slicing plane and the triangular faces because the STL model is composed of many triangular faces. First, the triangular faces whose three vertices are not on one side of the slicing plane δ are extracted. Then, the extracted triangular faces are intersected with the slicing plane δ to obtain the boundary line 1 constituting the boundary of the small forming angle surface, which is shown by the dotted line in Fig. 4.

3) Small forming angle surface generation

First, the boundary line of the small forming angle surface to be generated is extracted, and then it is triangulated to generate the small forming angle surface corresponding to each large forming angle area. To this end, the boundary line of the TLF (boundary line 2) between two points of BG is obtained by extracting the overlapping part of the boundary line of the difficult-to-form area and the boundary line of the TLF. And then the boundary line 1 and the boundary line 2 are combined to obtain the boundary line for generating the small forming angled surface (Fig. 4).

The triangular patches are generated by zoning the area that is surrounded by the boundary line to ensure that the forming angle of the generated small forming angle surface is less than θ_δ. In this method, the boundary line needs to be segmented first. The boundary line of the small forming angle surface is divided into four sections here: GJ, JJ', J'B and BG. Points B and G are known, and points J and J' can be determined by the following method.

① Select the point G on the boundary line 1 and its adjacent

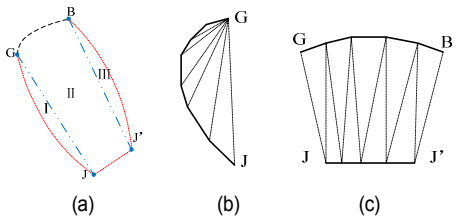

Fig. 5. Triangulation: (a) zoning; (b) zones I and III; (c) zone II.

point G' that is closest to the point G, and calculate the vector $\boldsymbol{l}_{GG'}$ at the same time.

② Extract the point T from the boundary line GJJ'B in the direction G→J and take the point T as one of vertices of the triangular face, and calculate the vector $\boldsymbol{l}_{GT}$.

③ Calculate the normal vector $\boldsymbol{n}_{\Delta}=\boldsymbol{l}_{GG'}\times\boldsymbol{l}_{GT}$ of triangular face composed of point G, G' and T by using the vector $\boldsymbol{l}_{GG'}$ and $\boldsymbol{l}_{GT}$, and also calculate the forming angle of the triangular face according to Eq. (2).

④ Judge whether the forming angle is greater than θ_{δ}. If the forming angle is greater than θ_{δ}, repeat the steps ① and ②, otherwise the point T is taken as the boundary point J. (The method of determining the point J' is the same.)

The area surrounded by the boundary line is divided into zone I (GJG), zone II (GJJ'BG) and zone III (BJ'B) by the dividing points, as shown in Fig. 5(a). Among them, the triangulation is made for zones I and III as shown in Fig. 5(b), that is, taking the point G as a fixed point and sequentially selecting the endpoints of each line segment on the GJ (solid line) to generate the triangular patch. The boundary lines at the top and bottom of the zone II are not in the same plane. So when constructing the triangular patches, GB and JJ' are first subdivided further, and then the triangular face is constructed by alternately taking the points up and down, as shown in Fig. 5(c). Finally, a small forming angle surface for a large forming angle surface is generated through these ways. With the method for the generation of the small forming angle surfaces based on the area zoning, the forming angles of zones I and III can be ensured to be θ_{δ}. And since the surface generated for the zone II is below the slicing plane δ and the forming angles of the triangular faces on the edges of both sides of the zone II have been made to be smaller than θ_{δ} when the boundary line is segmented, which guarantees that the forming angles of the zone II are smaller than θ_{δ}.

3.1.3 Synthesis of small forming angle surface and easy-to-form surface

First, the triangular face is divided according to the positional relationship between the slicing plane δ and the triangular face on easy-to-form surface. Their positional relationship can be divided into two types as shown in Fig. 6. The type 1 shown in Fig. 6(a) is that the vertices are all on one side of the slicing plane δ, which can be further divided into above the slicing plane δ and below the slicing plane δ. The type 2 shown in Fig. 6(b) is that the vertices are located on both sides of the

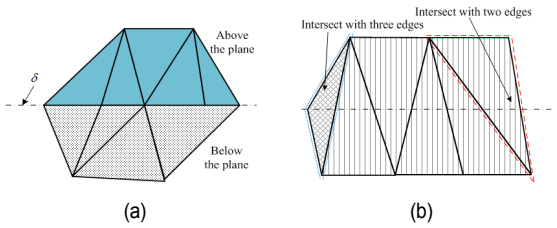

Fig. 6. Types of triangular faces: (a) type 1; (b) type 2.

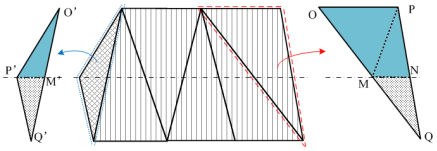

Fig. 7. The intersection of the triangular faces and the slicing plane.

slicing plane δ. The triangular faces that have an intersection with the slicing plane δ are extracted and saved according to the types 1 and 2, and the remaining triangular faces are divided into two categories and saved separately according to two cases of the type 1. The method for judging whether the point is above or below the slicing plane δ is to substitute the point into the plane equation. If the calculated result is greater than 0, it is above the plane, and if less than 0, it is below the plane.

Then, the intersection point of the extracted triangle faces of type 2 and the slicing plane δ is calculated and the triangle face is divided after slicing. The intersections between the triangular patch and the slicing plane are also divided into two cases, which are the intersection with two edges and the intersection with three edges, as shown in Fig. 6(b). For case 1 (intersection with two edges), the reconstruction and zoning are performed in the way of ΔOPQ in the dashed frame of Fig. 7. The ΔOPQ is divided into the quadrilateral OMNP and the ΔMNQ after being cut by the slicing plane. And the ΔMNQ is saved as a lower triangular face, and the quadrangle is split into two triangles that are saved to the upper triangular face. At this time, the ΔOPQ is reconstructed into three small triangular faces which are simultaneously divided into two categories shown in Fig. 6(a). For case 2 (intersection with three edges), the reconstruction and zoning are performed in the way of ΔO'P'Q' in the dotted frame of Fig. 7. The ΔO'P'Q' is divided into an upper ΔO'P'M' and a lower ΔQ'P'M' after being cut by the slicing plane. And then the divided triangles are saved in two categories shown in Fig. 6(a).

Finally, the triangular faces above the slicing plane in the easy-form-surface are extracted and saved in the same linked list as the first-stage forming model with the small forming angle surface generated by triangulation.

3.2 Generation of the first-stage toolpath

The first-stage toolpath is obtained by slicing the TLF using the equidistant horizontal plane with a spacing of Δh. Since

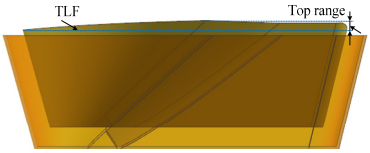

Fig. 8. The top range of the TLF.

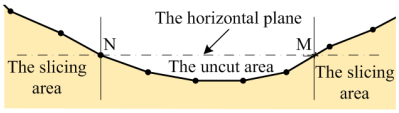

Fig. 9. The positional relationship between the point on the boundary ring and the horizontal slicing plane.

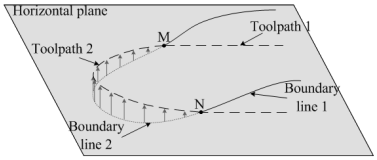

Fig. 10. Toolpath completion based on the projection method.

there are horizontal triangular faces at the bottom of the first-stage forming model, the triangular faces with a forming angle (relative to the horizontal plane) of 0 in the first-stage forming model are first removed to prevent errors when slicing to the bottom of the first-stage model with the horizontal plane. In addition, the height of the top of the TLF is inconsistent due to the different forming angles of the model at different places. The larger the forming angle is, the lower is the height of the TLF, and vice versa, which is shown in Fig. 8. The top range is defined as the range from the highest point to the lowest point on the top boundary ring of the TLF.

To prevent the problem of discontinuous toolpath during the top surface slicing and too deep squeezing of the first time, the uncut area at the top is judged by analyzing the positional relationship between the points on the top boundary ring of the TLF and the horizontal slicing plane when the slicing of the top area is performed.

When the points on the top boundary ring are above the horizontal slicing plane that is shown in Fig. 9, it means that this area belongs to the area to be cut and the tool location point of the current area can be obtained by slicing the current area using the horizontal plane. When the point is below the horizontal slicing plane, it means that this area cannot be cut because it does not reach the height of the horizontal slicing plane, so the tool location point of the current area could not be obtained. The point is directly used as the boundary point when the point is in the slicing plane (such as point N). And when two adjacent points of the boundary ring are located on both sides of the horizontal slicing plane, the intersection point obtained by the intersection of the line segment and the horizontal plane is used as the boundary point (such as point M).

The toolpath is generated using the method shown in Fig. 10 after determining the boundary points M and N. The boundary

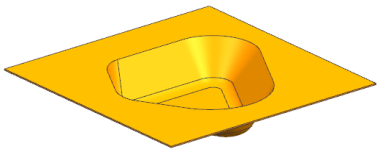

Fig. 11. The VWPIS model.

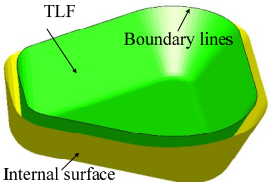

Fig. 12. The boundary line.

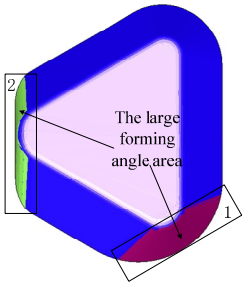

Fig. 13. Surface zoning.

line 2 (dotted line) on the left side of the MN is the boundary line of the TLF located in the uncut area, which is projected to the horizontal plane to obtain partial toolpath (toolpath 2) of the current slicing layer. And toolpath 1 for the area on the right side of the MN can be directly obtained through the slicing by using the horizontal plane. At this time, the toolpath of the current slicing layer can be obtained by combining the toolpaths (toolpath 1 and toolpath 2) of two regions.

Next, the toolpath that is not in the top range is directly obtained by the slicing of the horizontal plane after the top toolpath has been generated.

3.3 Algorithm application examples

The software platform for the generation of the first-stage forming model was established and the VWPIS model (Fig. 11) was selected as the test model to verify the correctness of the algorithm proposed above.

Fig. 12 shows the TLF obtained by offsetting the internal surface of the VWPIS model (Fig. 11) by a tool radius of 5 mm and the extracted boundary line of the TLF.

Fig. 13 shows the zoning of the TLF when the θ_{lim} is set to 55°. And the maximum forming angles of the area 1 and area 2 are 68.68° and 89.53°, respectively. Fig. 14 shows the slicing plane δ corresponding to the large forming angle regions, and its forming angle relative to the horizontal plane is θ_{δ} = 45°. Fig. 15 shows the zoning of the TLF after the easy-to-form area was cut by the slicing plane and the triangular faces were gen-

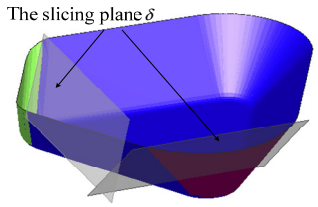

Fig. 14. Generation of the slicing planes.

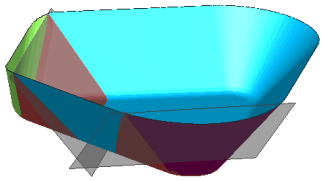

Fig. 15. Slicing the easy-to-form area.

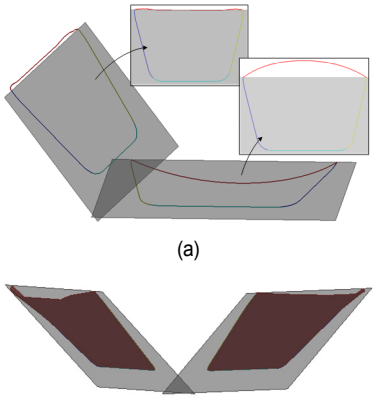

Fig. 16. Small forming angle surfaces: (a) boundary lines segmentation; (b) surfaces generation.

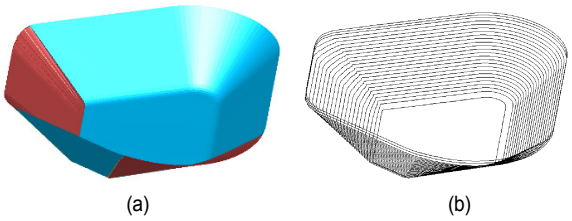

Fig. 17. First-stage forming: (a) first-stage forming model; (b) first-stage toolpath.

erated.

Fig. 16(a) shows the segmented boundary line of the small forming angle surface to be generated. Fig. 16(b) shows the small forming angle surface generated by triangulation based on the segmented boundary line. Fig. 17(a) shows the first-stage forming model obtained by synthesizing the small forming angle surfaces and the easy-to-form surface located above the slicing plane, and Fig. 17(b) shows the first-stage toolpath when the layer spacing is set to 1 mm.

4. Forming of unformed areas

4.1 Inclined plane generation for unformed independent features

After the first-stage forming, the unformed area includes the large forming angle surfaces and the easy-to-form surfaces located below the slicing plane δ. Among them, the easy-to-form surface below the slicing plane δ was divided and extracted when the first-stage forming model was constructed. At this time, it is only necessary to determine whether the large forming angle surface is connected with the unformed easy-to-form surface to perform one-to-one pairing synthesis to obtain multiple independent unformed features. Then, the appropriate inclined plane ε is selected for these independent unformed features to ensure that the forming angle of each triangular face on the feature relative to the inclined plane ε is less than the $\theta_{\lim}$. The specific method is as follows.

First, it is judged whether the forming angle of each triangular facet on the unformed independent feature relative to the inclined plane is less than the $\theta_{\lim}$, when the slicing plane δ determined in the previous chapter is used as an inclined plane. If it is so, the slicing plane δ can be directly used as the inclined plane ε. Otherwise, the inclined angle θ_ε of the inclined plane is determined through the enumeration method and the inclined plane ε by using Eqs. (1) and (3) (at this time, $t = \cos\theta_\varepsilon$). The inclination angle θ_ε whose range is 0° ~ 90° is enumerated from θ_δ to both sides at 1° intervals, and it can be determined whether the current enumerated plane can be used as the inclined plane ε by judging whether the forming angle of the triangular faces relative to the current enumerated plane is less than the $\theta_{\lim}$. If no suitable inclined plane is found through the entire range, the independent unformed features are spatially transformed to convert the slicing plane to a horizontal plane. And then the procedure of Sec. 3 is repeated for the current feature to continuously build the intermediate model as shown in Fig. 2(b) until the remaining independent unformed features can be enumerated to find the inclined plane.

4.2 Generation of the toolpaths for unformed areas

For the unformed independent features of which no inclined plane is found, the obtained intermediate model is sliced by using a series of equidistant planes (spacing is Δh) that are parallel to the slicing plane δ. However, because the inclined plane is not easy to determine and the process of slicing and intersecting is complicated, the spatial coordinate transformation method described in the previous section is used to transform the model into a coordinate system with the slicing plane δ as the horizontal plane. Then, the intermediate model is sliced by using the equidistant horizontal plane in the coordinate system to generate the tool location points. Finally, the inverse transformation is performed to transform the obtained tool location points into the points in the original coordinate

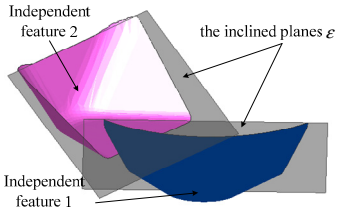

Fig. 18. The unformed independent features and the inclined planes.

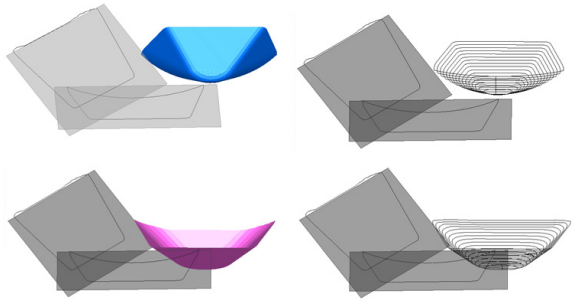

Fig. 19. The toolpaths: (a) unformed independent features after the posture adjustment; (b) horizontal toolpaths.

system so as to generate the inclined toolpath relative to the slicing plane δ.

Slicing the unformed independent features whose inclined plane ε has been found using a series of equidistant planes (spacing is Δh) parallel to the inclined plane ε. And the unformed independent features are transformed into the coordinate system with the inclined plane ε as horizontal plane using the spatial coordinate transformation method described in the previous section. Then, the tool location points are calculated by slicing the unformed independent features using the horizontal plane equidistant slicing in this coordinate system. Finally, the inverse transformation is performed to obtain the tool location points in the original coordinate system so as to generate the inclined toolpath of the current independent feature, which is relative to the slicing plane ε.

4.3 Algorithm application examples

The algorithm mentioned above was implemented based on the software system of the first-stage forming, and the VWPIS model (Fig. 11) was selected as the test object. Fig. 18 shows the unformed independent features after the first-stage forming and inclined planes ε of them determined by enumeration. The angle between the inclined planes and the horizontal plane of unformed independent features 1 and 2 is 45°.

Fig. 19(a) shows the unformed independent features after being transformed into a coordinate system with the inclined planes ε as the horizontal plane. Fig. 19(b) shows the toolpaths obtained by slicing each unformed independent feature horizontally with a layer spacing of 1 mm under the current coordinate system.

Fig. 20 shows the toolpaths for unformed areas obtained by

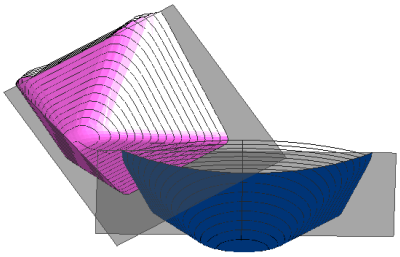

Fig. 20. The toolpath for unformed areas.

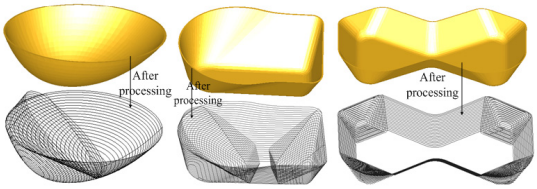

Fig. 21. The algorithm application examples of other models.

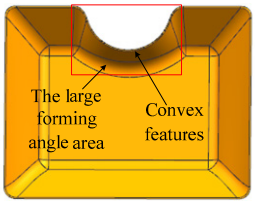

Fig. 22. The vertical-wall with convex features.

inversely transforming the above mentioned toolpaths. Meanwhile, some other case studies were given by taking other VWPIS models as examples to verify the robustness of the algorithms and program, and the results are shown in Fig. 21.

However, the method proposed in this paper also has certain limitations. It is impossible to generate a small forming angled surface that does not interfere with the part when the vertical-wall with convex features is included in the part as shown in Fig. 22, so that the subsequent processing cannot be performed.

5. Finite element analysis

In this section, the VWPIS model in Fig. 11 was selected to prove the effectiveness of the SMTPIF through finite element analysis of the distribution of thickness and strain by adopting the LS-DYNA software. To this end, finite element analysis of the two point incremental forming (TPIF) with one-stage and the typical multi-stage two point incremental forming (MTPIF) with two-stages was also carried out to compare with the SMTPIF. And the first-stage forming of the MTPIF adopted the toolpath is displayed in Fig. 17, and the second stage forming adopts the toolpath of one-stage forming.

In the finite element analysis, the unit type of the sheet was set to shell 163 that adopted the “Belytschko-Wong” algorithm, and the size of the sheet was 160 mm×160 mm×0.88 mm. The unit type of the support and the forming tool was set to solid 164, where the forming tool diameter was 10 mm. The material

Table 1. Material mechanical parameters of parts.

Part	Material	Density [kg · m^{-3}]	Elastic modulus [Gpa]	Poisson's ratio	Yield stress [Mpa]	Tangent modulus [Gpa]	Hardening coefficient
Sheet	Al1060	2700	55.94	0.324	153.6	2.9	0.19775
Tool	GCr15	8160	218	0.30	----	----	-----
Support	W6Mo5Cr4V2	7810	212	0.29	----	----	-----

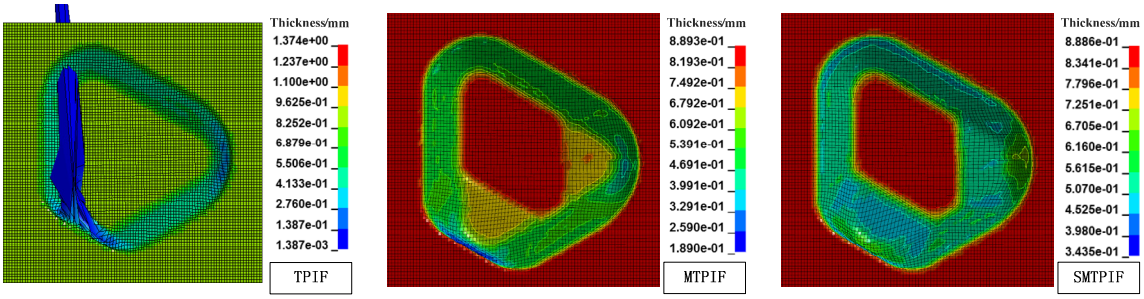

(a) (b) (c)

Fig. 23. Cloud figure of thickness distribution: (a) TPIF; (b) MTPIF; (c) SMTPIF.

mechanical parameters listed in Table 1 that are adopted in Zhu et al. [20] were used in the finite element analysis listed. The mesh of the sheet adopted the quadrilateral mapping mesh of 1.5 mm size, and the mesh of the tool and the support adopted the free tetrahedral mesh with the sizes 1.5 mm and 4 mm, respectively.

Because the VWPIS model has a vertical-wall with forming angles of 89.53°, the thickness of some meshes was reduced to 0.09586 mm when the numerical simulation based on the TPIF was performed to a depth of 15.17 mm. Then some meshes were distorted and the simulation failed when the simulation was performed to 21.62 mm depth, as shown in Fig. 23(a). For the MTPIF and the SMTPIF, the simulation results show that the sheet metal parts could be successfully formed. The thickness distributions of the MTPIF and SMTPIF are displayed in Figs. 23(b) and (c). Compared with the MTPIF, the numerical simulation results under the SMTPIF method are more ideal, and the thickness is distributed in a range of 0.3435 mm-0.8886 mm, while the thickness of the sheet part under the MTPIF method is distributed in a range of 0.1890 mm-0.8893 mm. At the same time, it can be found from Fig. 23 that the thickness of the part formed by the SMTPIF is not excessively thinned in the large forming angled areas.

By observing the deformation of the cell grid in Fig. 23, it can also be found that the longitudinal deformation of the mesh of the SMTPIF is smaller than that of the MTPIF in the area with large forming angles. To analyze the strain of parts formed by SMTPIF and MTPIF, the first, second, and third principal strain distribution cloud figures of parts were extracted as displayed in Fig. 24. From Fig. 24, in areas 1 and 2, the first principal strain of the sheet metal part formed with the MTPIF is greater than the part formed with the SMTPIF, and its first principal strain is mainly distributed on the side wall, while the first principal strain of the part under the SMTPIF is mainly distributed on the sidewall and bottom of sheet. In the SMTPIF, there are larger first and third principal strains on the top of the side wall of the area 2 for the sheet. And in the MTPIF, there are larger first and third principal strains on the entire side wall of the area 2, resulting in a smaller thickness in these areas. There are obvious second principal strains in areas 1 and 2 of the sheet metal under the two forming methods, and the second principal strain in the SMTPIF method is greater than that of the MTPIF. But the part thickness is not greatly thinned in the area where the second principal strain exists because of the relatively smaller first principal strain in this area.

To further analyze the mesh deformation of the MTPIF and SMTPIF, the strain-time curves of the meshes S26945, S29424, and S29911 in Fig. 24 were exported as displayed in Fig. 25. Meanwhile, Fig. 25 also shows the initial shape of mesh when it was not deformed and the deformation of each mesh after final forming. It can be seen from the figure that the deformation of each grid is similar in the first-stage forming, which are mainly the first and third principal strains. And the strain of S29424 is smaller than S26945 and S29911 because of the smaller forming angle of the first-stage forming model at S29424.

In the second-stage forming of the MTPIF, the second deformation of S26945 is very obvious, which shows that the first and third principal strains are further increased and a more obvious second principal strain appeared. Although S29911 is subjected to secondary extrusion, there is no obvious second deformation. While S29424 located in the bottom is not subjected to secondary extrusion, so there is no obvious secondary deformation.

In the second-stage forming of the SMTPIF, the secondary deformation of S26945 and S29424 is obvious. Among them, the mesh S29424 continues to be elongated with the first principal strain of S29424 being further increased, which results in

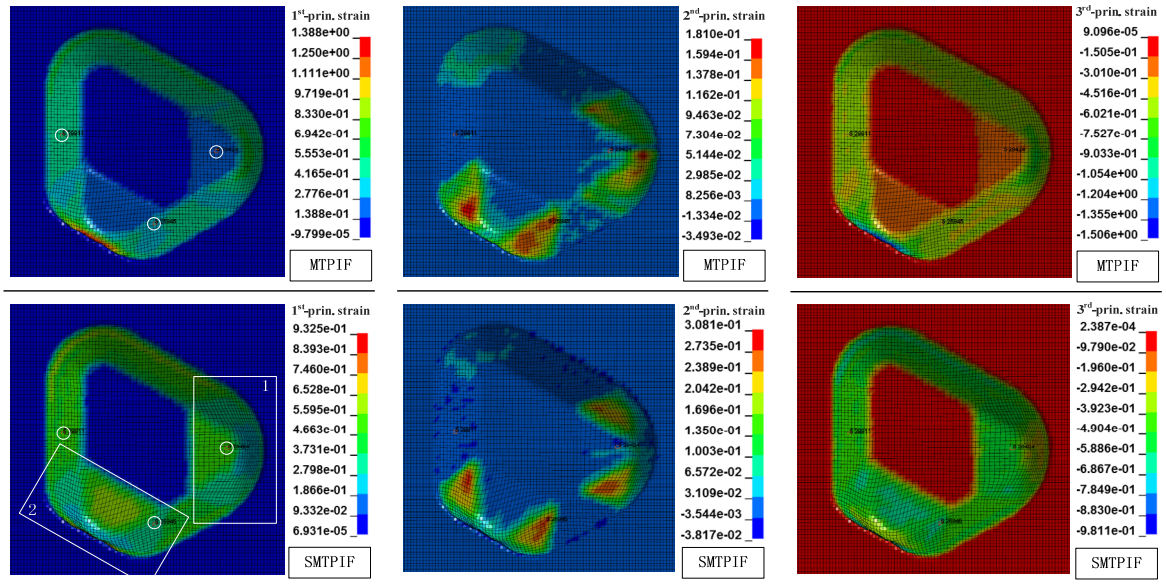

(a) (b) (c)

Fig. 24. Cloud figure of strain distribution: (a) 1st-prin. strain; (b) 2nd-prin. strain; (c) 3rd-prin. strain.

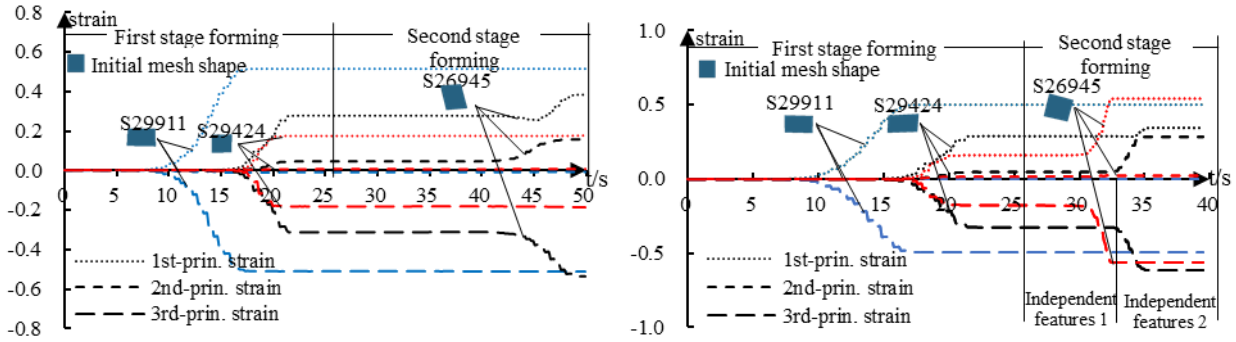

(a) (b)

Fig. 25. The strain-time curves: (a) MTPIF; (b) SMTPIF.

a decrease in thickness. And the mesh S26945 is widened with the second principal strain of S26945 increased significantly, which also results in a decrease in thickness. Compared with S26945 and S29424, the S29911 mesh located on the small forming angle surface does not incur secondary deformation, which also embodies the characteristics of the proposed method that forms the small forming angle surface and the vertical-wall by using one stage forming and multiple stages forming, repetitively.

By comparing the mesh deformation, compared with the MTPIF forming method, the SMTPIF forming method can make the entire inclined sheet surface after first-stage forming to participate in the second stage forming and to occur the secondary deformation. At the same time, the stretching of sheet by the extrusion is no longer same as the continuous downward stretching of the MTPIF because of the tilted tool-path; thus, the phenomenon of bottom sinking is reduced.

In summary, the SMTPIF can form the VWPIS that cannot be formed by the TPIF, and the sheet thickness reduction rate in

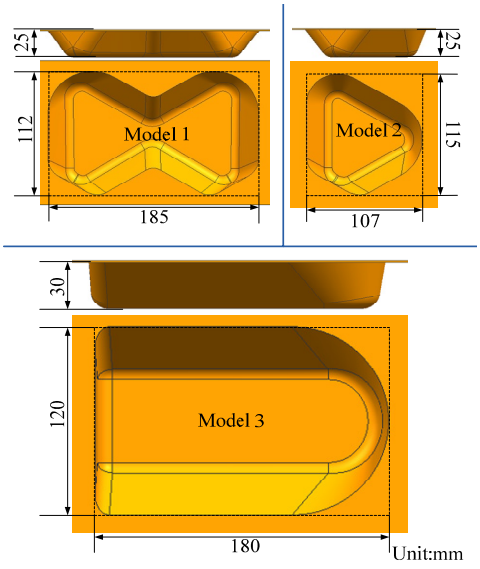

Fig. 26. The experimental model.

Table 2. Forming time of three models.

Type	TPIF	MTPIF	SMTPIF
Forming time [hour]	1.10 / 0.87 / 1.22	2.19 / 1.67 / 2.24	1.60 / 1.22 / 2.11

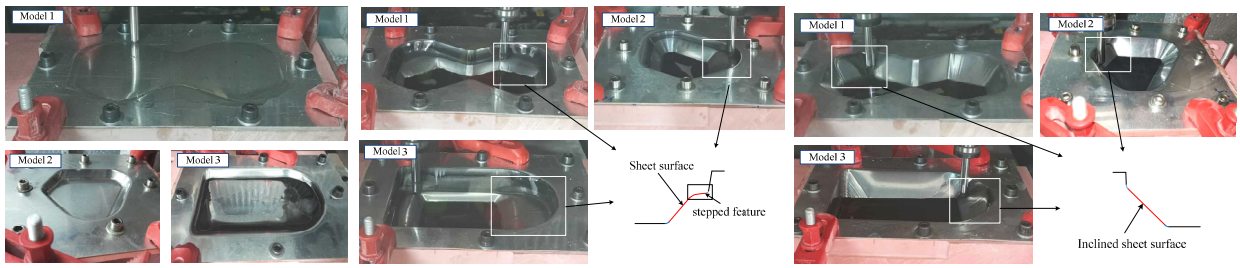

Fig. 27. The experiment: (a) TPSF; (b) MTPIF; (c) SMTPIF.

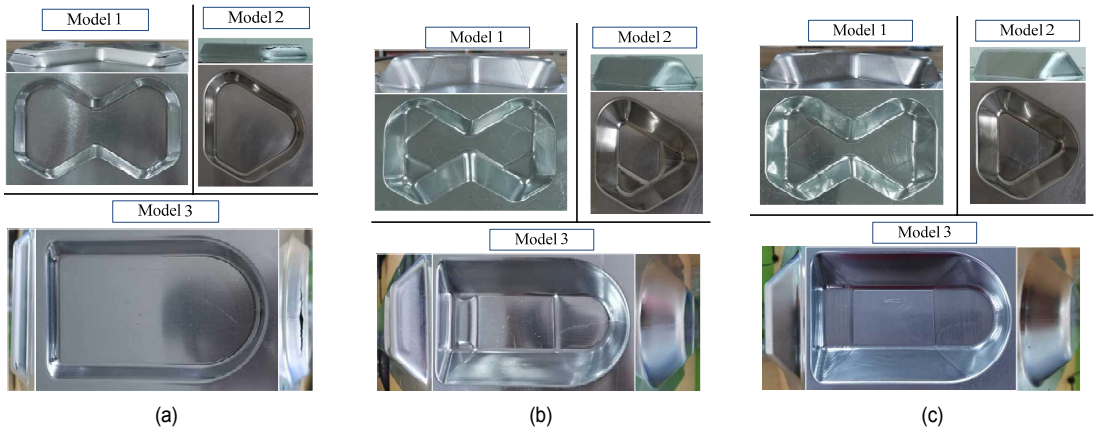

Fig. 28. The formed sheet metal parts: (a) TPIF; (b) MTPIF; (c) SMTPIF.

the large forming angle area is significantly reduced compared with the MTPIF forming method, which verifies the feasibility of the proposed method.

6. Experiment

A comparative experiment of the TPIF, the MTPIF and the SMTPIF was conducted with three different models as shown in Fig. 26. The Al1060 with a thickness of 0.88 mm and a hemispherical tool with diameters of 10 mm were adopted as experimental sheet and forming tool, respectively. The spindle speed, feed rate and layer distance were set as 400 r/min, 600 mm/min and 0.2 mm that were same as the corresponding parameters of the Zhu et al. [20], respectively. The θ_δ and θ_{lim} were set as 45° and 55°, respectively.

Then, the toolpaths of the three forming methods were imported into the CMICO software to calculate the forming time, as shown in Table 2. As can be seen from data in the table, since the SMTPIF does not perform secondary extrusion on the easy-to-form surface, it requires less forming time and has higher forming efficiency than the MTPIF that performs a two stage forming process. Compared with MTPIF, it can be seen that the SMTPIF reduces the processing time of models 1, 2, and 3 by 26.7 %, 26.9 % and 5.8 %, respectively, from Table 2. For model 3, the processing time was affected by the proportion of the straight wall on the side wall and the area involved in the forming of the bottom, so its processing efficiency is not improved significantly. But the forming efficiency will be significantly improved when the proportion of the side wall is small and the area participating in deformation at bottom is less, such as models 1 and 2.

Fig. 27 shows the forming process of the three forming methods. The stepped feature occurred during the second stage forming in the MTPIF, while the stepped feature did not occur in the SMTPIF. And this stepped feature will be evolved into a serious bulge with increasing of vertical-wall area, which appears at the bottom of the model, such as model 3 shown in Figs. 27(b) and 31(b). Meanwhile, the sheet metal was tilted under the squeezing of inclined toolpath in the second stage forming of the SMTPIF.

Fig. 28 shows the parts obtained by the TPIF, the MTPIF and the SMTPIF, respectively. The forming experiment based on the TPIF failed since the crack occurred in the large forming angle area when the forming depth of TPIF was about 12 mm.

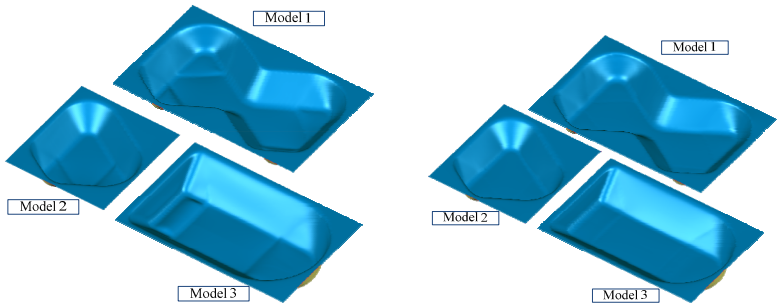

(a) (b)

Fig. 29. The surface contour of models: (a) MTPIF; (b) SMTPIF.

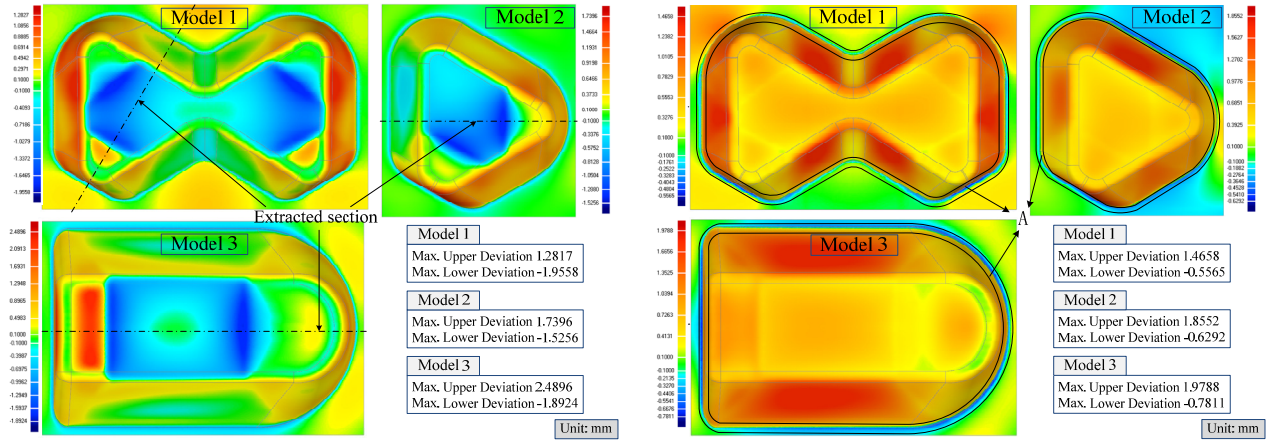

(a) (b)

Fig. 30. 3D contour deviation distribution cloud figure: (a) MTPIF; (b) SMTPIF.

However, both MTPIF and SMTPIF had successfully formed the parts. And overall flatness of the parts obtained using SMTPIF was better than that of MTPIF from the side view and top view of the sheet metal parts.

Due to the forming failure of the TPIF method, only the sheet metal parts obtained by the MTPIF and the SMTPIF were analyzed. The SMTPIF compared to the MTPIF, the contour dimensional accuracy and thickness are selected as the evaluation criteria to analyze the formed sheet metal parts. The Hexagon 3D coordinate measuring machine was used to scan the internal surface contour of the parts layer by layer, and the measurement interval was set to 2 mm. The measurement data was imported into Geomagic Studio/Qualify to obtain the 3D contour of parts shown in Fig. 29.

The measured contour data was used to calculate the 3D contour deviation from the theoretical CAD model. The 3D contour deviation distribution cloud figures of the parts under MTPIF and SMTPIF were obtained (the positive value represents that the formed sheet part was located above the theoretical CAD model, and the negative value represents that it was located below the theoretical CAD model) shown in Fig. 30. The bottom surface of the part formed by the MTPIF was obviously sinking, which resulted in a larger negative deviation at the bottom compared to the SMTPIF.

Because the deformation at the top edge of the sheet was mainly bending deformation, the sheet metal was rounded in this area (Area A in Fig. 30(b)). This area was also the main manifestation area of negative deviation of the SMTPIF method. Except for the rounded corner area (Area A), the sheet metal parts formed by the SMTPIF were mainly manifested as positive deviations caused by springback, and the maximum deviation was manifested in the planar feature of the side wall. In the MTPIF forming method, the contour deviation of the sheet metal part was reduced after the second extrusion in this area, which means that the second extrusion of the sheet can reduce the contour deviation caused by the springback.

The difference of the sinking phenomenon between the MTPIF and the SMTPIF can be seen from the sectional contour deviation distribution figure of model 2 and model 3 as shown in Fig. 31. In MTPIF, the largest negative deviation appeared at the junction between the deformed and undeformed area on the bottom, which indicates that the largest sinking had occurred in this area. And an obvious bending deformation appeared in the area B of bottom participating in forming in the part formed by the MTPIF. This is because in the second stage forming of the MTPIF, the easy-to-form area has a supporting effect on the sheet of area B, while the forming tool has a

Table 3. Contour measurement data (unit: mm).

Type	3D deviation		2D deviation	
	MTPIF	SMTPIF	MTPIF	SMTPIF
	Model 1 / 2 / 3	Model 1 / 2 / 3	Model 1 / 2 / 3	Model 1 / 2 / 3
Max +	1.2827 / 1.7397 / 2.4896	1.4658 / 1.8552 / 1.9788	0.7300 / 0.7297 / 2.4164	1.4092 / 1.0837 / 1.1417
Max -	-1.9457 / -1.5256 / -1.8924	-0.5565 / -0.6292 / -0.7811	-1.6231 / -1.5142 / -1.8885	-0.4804 / -0.2179 / -0.7631
Average +	0.3490 / 0.3841 / 0.5211	0.5702 / 0.6579 / 0.7790	0.3222 / 0.4313 / 0.8753	0.5759 / 0.6265 / 0.7362
Average -	-0.5041/ -0.3194 / -0.4584	-0.0926 / -0.1981 / -0.2523	-0.8106 / -0.5408 / -0.5526	-0.2610 / -0.0859 / -0.3232

Table 4. Thickness measurement data at straight wall of models 2 and 3 (unit: mm).

Type	Model 2		Model 3	
	MTPIF	SMTPIF	MTPIF	SMTPIF
Min thickness	P58:0.131	P60:0.367	p11:0.170	p9:0.377
Average thickness	P54-P63:0.348	P54-P63:0.552	p1-p14:0.432 p98-p111:0.415	p1-p14:0.558 p98-p111:0.689

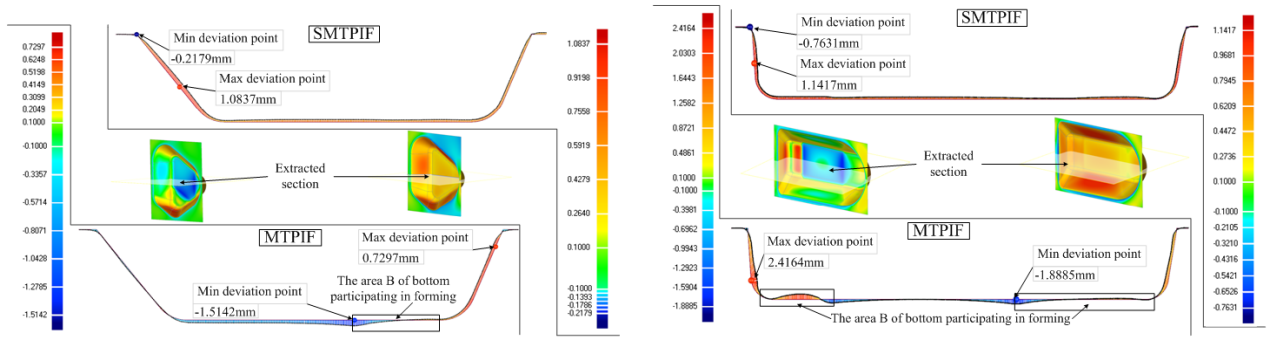

Fig. 31. Section contour deviation: (a) model 2; (b) model 3.

downward force on the area in the forming process, which causes the sheet to be bent and deformed. Meanwhile the bottom does not sink excessively because of the supporting effect of the easy-to-form area. In the SMTPIF, there is no sinking at the bottom of the part and its bottom is relatively flat. The main source of error is caused by the spring back of the sheet metal. The contour measurement data of each forming part is shown in Table 3.

To obtain the sheet thickness on the section passing through the vertical-wall of model 2 and model 3, the parts were cut by a wire cutting machine at the position shown in Fig. 32. Then the sheet thickness on the cutting sections was measured and the sectional thickness curves were drawn as shown in Fig. 32. The thickness measurement data at straight wall of models 2 and 3 is shown in Table 4.

From the slicing sections and the section thickness distribution curves, there is little difference between the two forming methods on the easy-to-form area (P1-P16) and the unformed areas of the bottom (P16-P38 and p30-p67). In the vertical-wall areas (P53-P63, p1-p15 and p97-p111), the minimum thickness of models 2 and model 3 formed by the MTPIF is 0.131 mm and 0.17 mm, respectively, while the minimum thickness by the SMTPIF is 0.367 mm and 0.377 mm. The thickness of the bottom surfaces (P38-P53, p15-p30 and p67-p97) that participate in the forming based on the MTPIF is thicker than that based on the SMTPIF, which shows that although the MTPIF forming method makes the surface of the bottom to participate in the forming, the degree of participation is significantly less than that of the SMTPIF.

In the SMTPIF, the metal material of the areas (P38-P53, p15-p30 and p67-p97) participates in the forming so that the metal material flows to the areas (P53-P63, p1-p15 and p97-p111) and makes up the lack of material in the areas (P53-P63, p1-p15 and p97-p111), which makes the thickness of the areas (P53-P63, p1-p15 and p97-p111) not to be excessively thinned and the thickness uniformity to be promoted. Compared with MTPIF, it can be seen that the minimum thickness of models 2 and 3 formed by SMTPIF increased by 180.1 % and 121.8 %, respectively, and the average thickness improved by 58.6 % and 29.2 % (66.0 % at p98-p111) from Table 4. According to

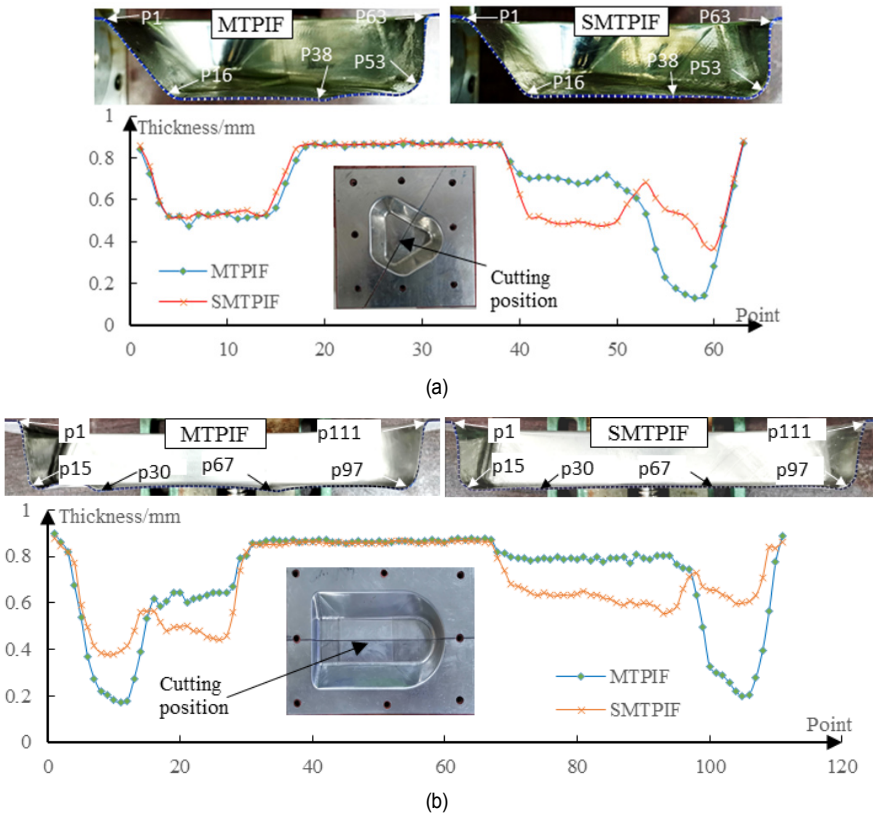

Fig. 32. Section thickness distribution curve: (a) model 2; (b) model 3.

the uniformity of the overall thickness distribution and the thickness difference, the SMTPIF is significantly better than the MTPIF, which verifies the effectiveness of the proposed method.

7. Conclusions

A selective MTPIF based on the forming angle was proposed in this paper. It can be seen from the comparative analysis with the TPIF, MTPIF and SMTPIF, the VWPIS had been successfully formed by using the MTPIF and the SMTPIF, while failed in the TPIF. With the FE analysis and experiment, the effectiveness of the proposed method was verified, and some important conclusions are summarized as follows.

i) The algorithm application examples show that the software platform written by the method proposed in the present work can realize the generation of the intermediate model of VWPIS and the corresponding forming toolpath.

ii) Since the SMTPIF selectively adopts multi-stage incremental forming only for the difficult-to-form surfaces with large forming angles, it can save forming time for models 1, 2 and 3 by 26.7 %, 26.9 % and 5.8 %, respectively.

iii) Because the inclined tool path is used in the second stage forming, there are no step features in SMTPIF, so that the formed sheet parts, of which the bottom contour error is expressed as a positive error caused by springback (around 0.6 mm for models 1 and 2, and around 0.8 mm for model 3), have a better surface contour. However, the sheet metal formed by MTPIF has a sinking problem that seriously affects the contour accuracy at the bottom. The contour error at bottom of the parts is expressed as a negative deviation caused by sinking (around -1.6 mm, -1.4 mm and -1.8 mm for models 1, 2 and 3, respectively) and the positive deviation caused by sheet bending (around 0.5 mm, 0.2 mm and 2 mm for models 1, 2 and 3, respectively).

iv) In addition, the proposed method can make the surfaces with different forming angles to be given different forming strategies and forming parameters so that more sheet metal can participate in the forming deformation in a better way, which can be seen from the FE analysis, thereby reducing the thickness of the vertical-wall surface and obtaining better thickness distribution. Compared with MTPIF, the minimum thickness of models 2 and 3 formed by SMTPIF increased by 180.1 % and 121.8 %, respectively.

In the present work, the SMTPIF, a method combining multi-stage forming and inclined toolpath has achieved no-sinking and relatively low-thinning forming for VWPIS. In the follow-up study, the effect of secondary pressing of the tool on the contour dimensional accuracy in the SMTPIF is necessary to be researched to improve the accuracy of contour.

Compliance with ethical standards

The authors declare that they have no conflict of interest.

Nomenclature

θ_{lim}	: Forming limit angle
θ_i	: Forming angle of the *i*-th triangular face
δ , ε	: Inclined plane
θ_δ , θ_ε	: Inclined angle of the inclined plane
$\boldsymbol{l}_{BG}$, $\boldsymbol{l}_{GG'}$, $\boldsymbol{l}_{GT}$	: Direction vector of the straight line
$\boldsymbol{n}_\delta$, $\boldsymbol{n}_o$, $\boldsymbol{n}_\Delta$	: Normal vector of the plane
Δh	: Spacing of the equidistant horizontal plane

References

[1] T. J. Kim and D. Y. Yang, Improvement of formability for the incremental sheet metal forming process, *Int. J. Mech. Sci.*, 42 (7) (2000) 1271-1286.

[2] H. Iseki and T. Naganawa, Vertical wall surface forming of rectangular shell using multistage incremental forming with spherical and cylindrical rollers, *J. Mater. Process. Technol.*, 130-131 (2002) 675-679.

[3] G. Hirt, J. Ames, M. Bambach, R. Kopp and R. Kopp, Forming strategies and process modelling for CNC incremental sheet forming, *CIRP Ann-Manuf Technol.*, 53 (1) (2004) 203-206.

[4] M. Skjoedt, N. Bay, B. Endelt and G. Ingarao, Multi stage strategies for single point incremental forming of a cup, *Int. J. Mater. Form.*, 1 (1) (2008) 1199-1202.

[5] J. R. Duflou, J. Verbert, B. Belkassem, J. Gu, H. Sol, C. Henrard and A. M. Habraken, Process window enhancement for single point incremental forming through multi-step toolpaths, *CIRP Ann-Manuf Technol.*, 57 (1) (2008) 253-256.

[6] R. Malhotra, A. Bhattacharya, A. Kumar, N. V. Reddy and J. Cao, A new methodology for multi-pass single point incremental forming with mixed toolpaths, *CIRP Ann-Manuf Technol.*, 60 (1) (2011) 323-326.

[7] R. Lingam, A. Bansal and N. V. Reddy, Analytical prediction of formed geometry in multi-stage single point incremental forming, *Int. J. Mater. Form.*, 9 (2015) 395-404.

[8] E. Ndip-Agbor, P. Cheng, N. Moser, K. Ehmann and J. Cao, Prediction of rigid body motion in multi-pass single point incremental forming, *J. Mater. Process. Technol.*, 269 (2019) 117-127.

[9] K. Suresh, S. P. Regalla and N. Kotkundae, Finite element simulations of multi stage incremental forming process, *Mater. Today: Proceed.*, 5 (2, part 1) (2018) 3802-3810.

[10] M. J. Mirnia, B. Mollaei Dariani, H. Vanhove and J. R. Duflou, Thickness improvement in single point incremental forming deduced by sequential limit analysis, *Int. J. Adv. Manuf. Technol.*, 70 (9-12) (2014) 2029-2041.

[11] T. T. Cao, B. Lu, D. K. Xu, H. Zhang, J. Chen, H. Long and J. Cao, An efficient method for thickness prediction in multi-pass incremental sheet forming, *Int. J. Adv. Manuf. Technol.*, 77 (1-4) (2015) 469-483.

[12] X. Q. Li, K. Han and D. S. Li, Multi-stage two point incremental sheet forming, *J. Phys.: Conf. Ser.*, 1063 (1) (2018) 1-6.

[13] X. Q. Li, K. Han, P. Xu, H. P. Wang, D. S. Li, Y. L. Li and Q. Li, Experimental and theoretical analysis of the thickness distribution in multistage two point incremental sheet forming, *Int. J. Adv. Manuf. Technol.*, 107 (1-2) (2020) 191-203.

[14] Z. B. Liu, W. J. T. Daniel, Y. L. Li, S. Liu and P. A. Meehan, Multi-pass deformation design for incremental sheet forming: Analytical modeling, finite element analysis and experimental validation, *J. Mater. Process. Technol.*, 214 (3) (2014) 620-634.

[15] P. Gupta and J. Jeswiet, Design and development of an aerospace component with single-point incremental forming, *Int. J. Adv. Manuf. Technol.*, 103 (9-12) (2019) 3683-3702.

[16] S. Tanaka, Incremental sheet metal formed square-cup obtained through multi-stepped process, *Procedia. Manuf.*, 15 (2018) 1170-1176.

[17] S. Wu, Y. W. Ma, L. T. Gao, Y. X. Zhao, S. Rashed and N. S. Ma, A novel multi-step strategy of single point incremental forming for high wall angle shape, *J. Manuf. Process.*, 56 (2020) 697-706.

[18] B. Gianluca, G. Marco, F. Livan and M. Fabrizio, Multi-directional vs. mono-directional multi-step strategies for single point incremental forming of non-axisymmetric components, *J. Manuf. Process.*, 55 (2020) 22-30.

[19] P. P. Dai, Z. D. Chang, M. Li and J. Chen, Reduction of geometric deviation by multi-pass incremental forming combined with tool path compensation for non-axisymmetric aluminum alloy component with stepped feature, *Int. J. Adv. Manuf. Technol.*, 102 (1-4) (2019) 809-817.

[20] H. Zhu and L. T. Liu, Research the CNC incremental forming of straight-wall part based on a virtual auxiliary body, *J. Mater. Process. Technol.*, 288 (2020) 116841, https://doi.org/10.1016/j.jmatprotec.2020.116841.

[21] H. Zhu and J. L. Li, Research on the CNC incremental forming based on multidirectional real-time adjustment of the sheet posture, *Int. J. Adv. Manuf. Technol.*, 110 (5-6) (2020) 1339-1350.

[22] J. C. Li, J. J. Shen and B. A. Wang, A multipass incremental sheet forming strategy of a car taillight bracket, *Int. J. Adv. Manuf. Technol.*, 69 (9-12) (2013) 2229-2236.

Hu Zhu is a Professor in the College of Mechanical and Electrical Engineering at Shenyang Aerospace University. He received his B.S. from Jilin University, and M.S. and Ph.D. in the Department of Mechanical Design and Production Engineering at Seoul National University. His current research interests include CAD/CAM, 3D printing, CNC incremental forming.

Luteng Liu is currently an M.S. student in the College of Mechanical and Electrical Engineering at Shenyang Aerospace University. He received his B.S. from the Mechanical Manufacturing and Automation at Shenyang Aerospace University. His research interests include CAD/CAM, CNC incremental forming.

Yibo Liu is currently a Vice Professor in the Science and Technology Training Center at the Guidaojiaotong Polytechnic Institute. He received his M.S. from Shenyang Aerospace University. His research interests include CAD/CAM, CNC machining, and CNC incremental forming.

Jaeguan Kang is currently a Professor in the Division of Mechanical Engineering at the Kyungnam University. He received his Ph.D. from Pohang University of Science and Technology, M.S. from Korea Advanced Institute of Science and Technology, B.S. from Seoul National University. His primary research interests include CAD/CAM, Incremental sheet metal forming.